Seismic Design and Performance of Composite Coupling Beam-to-SpeedCore Wall Connections

Amit H. Varma, Mubashshir Ahmad, Soheil Shafaei, and Ron Klemencic

ABSTRACT

Coupled composite plate shear walls—concrete filled (CC-PSW/CFs) are an effective seismic lateral-force-resisting system for the design and construction of mid- to high-rise buildings around the world. The coupled system consists of two or more composite plate shear walls—concrete filled (C-PSW/CFs) connected to each other using composite coupling beams located at the story heights. The CC-PSW/CF system can provide higher overturning moment capacity, lateral stiffness, and ductility than uncoupled walls. Concrete-filled steel box sections are typically used for the composite coupling beams, which are designed to be flexure critical members. When the CC-PSW/CF system is subjected to lateral seismic forces, plastic hinge formation and inelastic deformations (energy dissipation) occur near the ends of most of coupling beams along the structure's height, followed by flexural hinging of the C-PSW/CFs, typically at the base. This paper presents the details and design of four composite coupling beam-to-C-PSW/CF connection configurations. Six connection specimens representing the four connection configurations, with beam clear span-to-section depth, L_b/d, ratios of 3.5 and 5.1, were designed and tested. The lateral force-displacement and moment-rotation responses of the specimens are summarized. All six composite coupling beam-to-C-PSW/CF wall connection specimens (1) developed and exceeded the plastic flexural capacities, M_p, of the coupling beams calculated using the plastic stress distribution method and (2) developed chord rotation capacities greater than 0.03 radian before their flexural strength degraded to 80% of the plastic moment capacity, M_p.

Keywords: SpeedCore, composite, connections, coupling beam, coupled system, shear walls, seismic design, experimental research, performance assessment.

INTRODUCTION

Coupled composite plate shear walls—concrete filled (CC-PSW/CF) consist of two or more composite plate shear walls (concrete filled) connected using composite coupling beams (links), as shown in Figures 1(a) and 1(b). The uncoupled C-PSW/CF system was included as a seismic force-resisting system (SFRS) in ASCE/SEI 7-16 (ASCE, 2016), and its seismic design and detailing requirements were presented in the 2016 AISC *Seismic Provisions for Structural Steel Buildings*, ANSI/AISC 341-16 (AISC, 2016). However, the coupled (CC-PSW/CF) system was not addressed in either standard.

Recent research has focused on developing seismic design and detailing requirements for the CC-PSW/CF system. The results from a rigorous FEMA P695 study conducted recently (Bruneau et al., 2019; Kizilarslan et al. 2021b; Broberg et al., 2022) have confirmed that CC-PSW/CF can be used as a distinct SFRS with seismic response modification factors of 8 ($R = 8$), overstrength factor of 2.5 ($\Omega_0 = 2.5$), and displacement amplification factor of 5.5 ($C_d = 5.5$). This led to the inclusion of the CC-PSW/CF system and its seismic design and detailing procedure in FEMA P-2082-1 (FEMA, 2020) and, subsequently, its seismic response modification factors in ASCE/SEI 7-22 (ASCE, 2022); seismic design and section detailing requirements in the 2022 AISC *Seismic Provisions for Structural Steel Buildings*, ANSI/AISC 341-22 (AISC, 2022a); and detailed design examples and guidance in AISC Design Guide 38, *SpeedCore Systems for Steel Structures* (Varma et al., 2023) and Chapter 5 of FEMA P-2192-V1 (FEMA, 2021).

Figure 1 shows a typical CC-PSW/CF system along with its components. Figure 1(c) shows a typical cross section of a planar C-PSW/CF. Planar C-PSW/CF comprises two steel web plates and two flange (closure) plates welded together to form a box section. The web plates are connected using tie bars, which improve the stability of empty steel modules during transportation, erection, and concrete casting (Varma et al., 2019). The steel tie bars and headed stud anchors are used to develop the composite interaction between steel plates and infill concrete. In the seismic design of CC-PSW/CF, composite coupling beams are used due to their high flexural stiffness and capacities. Figure 1(d) shows a typical cross section of a composite coupling beam made of built-up steel box-section and plain concrete.

Amit H. Varma, Karl H. Kettelhut Professor, Purdue University, West Lafayette, Ind. Email: ahvarma@purdue.edu (corresponding)

Mubashshir Ahmad, PhD Candidate, Purdue University, West Lafayette, Ind. Email: ahmad54@purdue.edu

Soheil Shafaei, Lead Research Scientist, Purdue University, West Lafayette, Ind. Email: sshafaei@purdue.edu

Ron Klemencic, President and CEO, Magnusson Klemencic Associates, Seattle, Wash. Email: rklemencic@mka.com

Paper No. 2022-11

The empty steel modules of C-PSW/CFs are prefabricated in a shop and transported to the site for erection. The empty steel modules of C-PSW/CFs serve as formwork and falsework during the construction and concrete casting; hence, using this system improves the construction schedule considerably (Varma et al., 2019). The steel plates act as primary reinforcement of the walls in the composite phase (Varma et al., 2014). This system is commercially referred to as the SpeedCore system by the American Institute of Steel Construction (AISC) because of the remarkable reduction in overall construction time. This decrease in construction time was demonstrated by the Rainier Square Tower (Traut-Todaro, 2019), constructed approximately 43% faster than the typical reinforced concrete (RC) corewall building with steel framing. The Rainier Square Tower is the first commercial high-rise building employing the CC-PSW/CF system in the United States. It utilized a CC-PSW/CF core system surrounded by traditional steel gravity frames (composite steel floor). The wall modules were preinstalled with shear tabs for steel beam framing connections and ledger angles for deck support. Holes were predrilled at the floor level to connect the concrete deck to the composite core through dowel rebars. The prefabricated steel modules were erected and spliced on site by a combination of partial-joint-penetration (PJP) groove welds and reinforcing fillet welds.

The coupling beam-to-composite wall connections are an integral part of the CC-PSW/CF system. Seismic performance requirements for these coupling beam-to-wall connections have been specified in ANSI/AISC 341-22. Performance confirmation for coupling beam-to-wall connections is essential to achieve the seismic performance of the system (Kizilarslan et al., 2021b; Broberg et al., 2022). This paper presents the design of four different beam-to-wall connection configurations in accordance with the corresponding provisions in ANSI/AISC 341-22, as exemplified

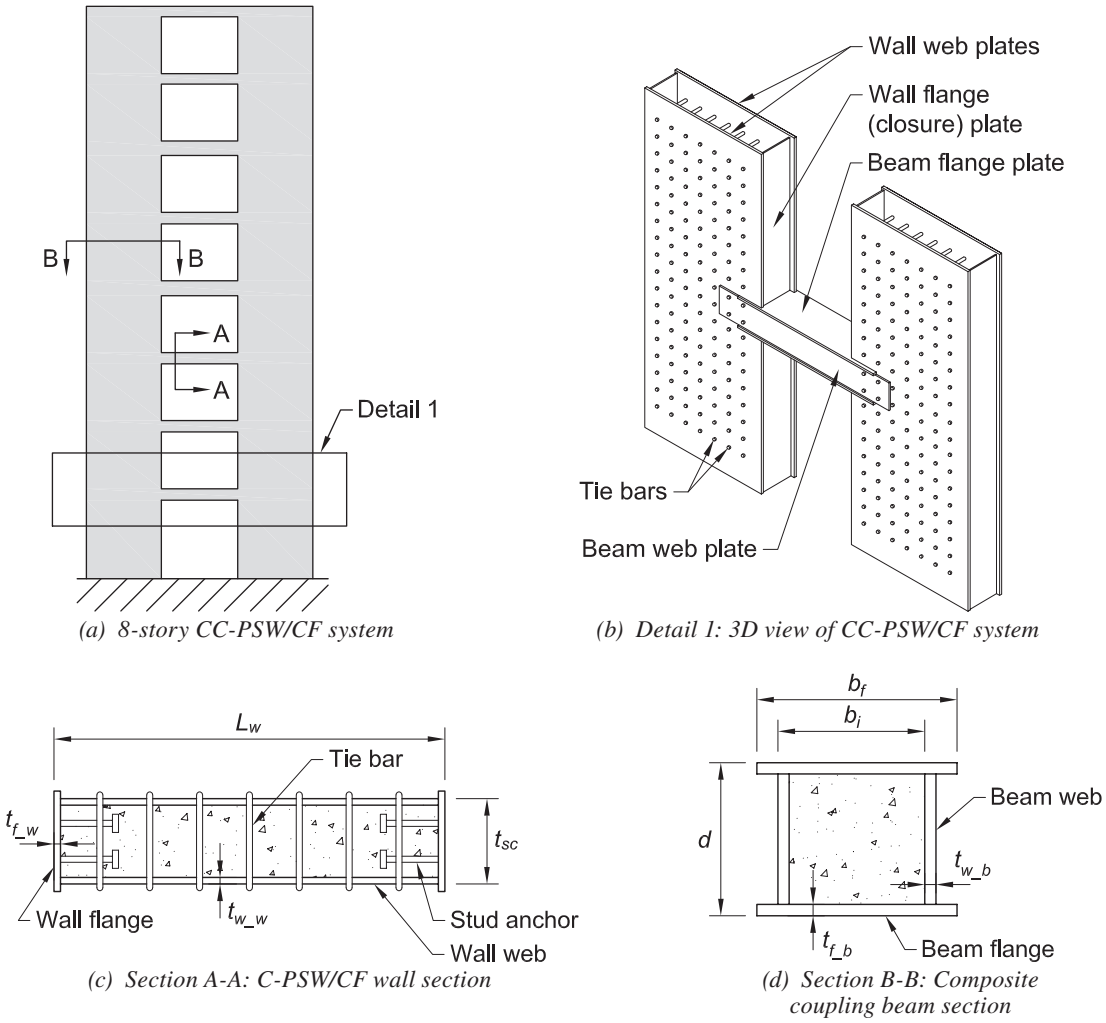

(a) 8-story CC-PSW/CF system

(b) Detail 1: 3D view of CC-PSW/CF system

(c) Section A-A: C-PSW/CF wall section

(d) Section B-B: Composite coupling beam section

Fig. 1. Typical CC-PSW/CF system and components.

in AISC Design Guide 38, and their experimental performance in terms of the rotational capacities developed.

BACKGROUND

Individual uncoupled shear walls provide good seismic behavior and resistance. However, connecting individual shear walls using coupling beams at each story provides greater stiffness and redundancy to the seismic force-resisting system. The coupled system has lateral stiffness greater than the sum of the two connected walls (El-Tawil et al., 2010). The overturning moment is resisted partially by coupling action resulting from the axial force (tension-compression) couple across the wall system, which reduces the moment demand on the individual walls. If designed appropriately, plastic hinging and inelastic deformations (energy dissipation) occur at the ends of the coupling beams and spread along the height of the structure, rather than just being concentrated at the base of the individual shear walls.

For the CC-PSW/CF system, Broberg et al. (2022) developed a capacity design method based on a weak beam–strong wall design principle that prioritizes the occurrence of plastic hinging at the ends of the coupling beams and spreading of plasticity along the height of the structure before forming plastic hinges at the bases of the individual shear walls. Several archetype (3- to 22-story) structures were designed using this capacity design principle. Nonlinear inelastic finite element models for the composite walls and coupling beams were developed and benchmarked using experimental results (Kizilarslan et al., 2021a; Shafaei et al., 2021a, 2021b; Bruneau et al., 2019). These models were used to conduct incremental dynamic (nonlinear time-history) analyses for 22 sets of appropriately scaled ground motions according to the FEMA P695 procedure. The seismic response of CC-PSW/CF systems reasonably follows the sequence of plastification assumed by the capacity design principle (Broberg et al., 2022). Statistical analysis of the results confirms the proposed seismic factors ($R = 8$, $\Omega_0 = 2.5$, and $C_d = 5.5$) for the CC-PSW/CF system (Kizilarslan et al., 2021b).

The coupled system has better ductility and seismic behavior due to the spread of plasticity along the height of the structure through the formation of plastic hinges at the ends of the coupling beams. For uncoupled walls, inelastic deformations concentrate in the plastic hinge regions at the base of the individual walls, while the remaining wall lengths remain mostly elastic. Comprehensive FEMA P695 studies conducted for uncoupled C-PSW/CF wall systems have confirmed seismic factor values of $R = 6.5$, $\Omega_0 = 2.5$, and $C_d = 5.5$ for the uncoupled system (Broberg et al., 2023; Kizilarslan and Bruneau, 2023).

The higher R factor of 8 for the coupled system acknowledges its better ductility and ability to spread plasticity along the height of the structure. The coupling beam-to-wall connections play an important role in achieving this system level ductility. They are required to have adequate strength to develop the flexural plastic hinges at the ends of the coupling beams and sustain them for at least 0.03 rad of chord rotation before flexural strength degrades below 80% of the nominal plastic moment capacity. The incremental dynamic (nonlinear time-history) analyses conducted as part of the FEMA P695 studies modeled the inelastic behavior of the coupling beam plastic hinges in accordance with this performance requirement, present in ANSI/AISC 341-22, Section H8.8.

Consequently, the coupling beam-to-wall connections used in the CC-PSW/CF system should accommodate this performance requirement and exhibit a minimum chord-rotation capacity of 0.03 rad before flexural strength degrades to 80% of the nominal plastic moment capacity, M_p. This type of connection performance requirement, shown in Figure 2, is prevalent in seismic design provisions (ANSI/AISC 341-22). For example, beam-to-column connections in intermediate moment frames and special moment frames are required to have chord rotation capacities of at least 0.02. and 0.04 rad, respectively.

It is also important to note that the FEMA P695 study and, consequently, the current seismic design provisions (ANSI/AISC 341-22) are limited to CC-PSW/CF systems designed with flexure-critical coupling beams, with a clear span-depth (L_b/d) ratio greater than or equal to 3 and less than or equal to 5. Shear-critical composite coupling beams with an L_b/d ratio less than 3.0 were not included for several reasons, including the inadequate cyclic performance seen in tests conducted by Nie et al. (2014). Currently, there is a lack of coupling beam-to-composite wall connections that have been designed, detailed, and then tested to confirm their performance under cyclic loading. This paper directly addresses this gap in knowledge.

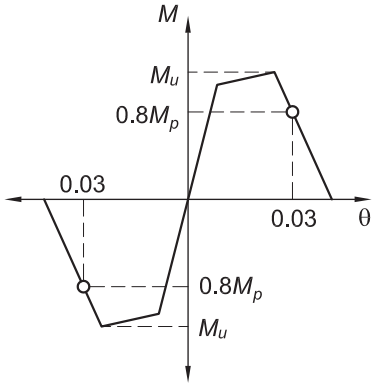

Fig. 2. Envelope of moment–rotation (M-θ) response of coupling beam.

Table 1. Planar CC-PSW/CF Archetypes from Bruneau et al. (2019)							
Case	Number of Stories	Coupled Wall Length, L_w, in.	Wall Thickness, t_{sc}, in.	Plate Thickness, t_{f_w}, and t_{w_w}, in.	Coupling Beam Length, L_b, in.	Coupling Beam Section, in.	L_b/d
PG-1A	8	144	20	9/16	72	$20(b_f)\times24(d)\times$ $3/8(t_{f\_b})$, $3/8(t_{w\_b})$	3
PG-1B		132	24	9/16	96	$24(b_f)\times24(d)\times$ $1/2(t_{f\_b})$, $3/8(t_{w\_b})$	4
PG-1C		120	24	5/8	120	$24(b_f)\times24(d)\times$ $1/2(t_{f\_b})$, $3/8(t_{w\_b})$	5
PG-2B	8	144	10	3/16	72	$10(b_f)\times18(d)\times$ $3/16(t_{f\_b})$, $1/4(t_{w\_b})$	4
PG-1D	12	204	18	9/16	72	$18(b_f)\times24(d)\times$ $5/16(t_{f\_b})$, $3/8(t_{w\_b})$	3
PG-1E		192	22	9/16	96	$22(b_f)\times24(d)\times$ $7/16(t_{f\_b})$, $3/8(t_{w\_b})$	4
PG-1F		180	24	9/16	120	$24(b_f)\times24(d)\times$ $1/2(t_{f\_b})$, $3/8(t_{w\_b})$	5
PG-2E	12	204	8	3/16	72	$8(b_f)\times18(d)\times$ $3/16(t_{f\_b})$, $1/4(t_{w\_b})$	4

DESIGN AND DETAILS OF CONNECTIONS IN ARCHETYPE STRUCTURES

Several CC-PSW/CF archetype structures (3-, 8-, 12-, 18-, and 22-story buildings) using planar or C-shaped C-PSW/CFs and composite coupling beams were designed following the capacity design method described in Broberg et al. (2022). Table 1 provides the dimensions and details of 8- and 12-story CC-PSW/CF archetype structures with planar C-PSW/CFs and composite coupling beams as shown in Figure 1 and reported in Bruneau et al. (2019) and Kizilarslan et al. (2021b).

Composite Coupling Beam-to-C-PSW/CF Connections

Four composite coupling beam-to-C-PSW/CF connections—identified as connection types 1, 2, 3, and 4—were developed based on construction considerations and expected structural performance. Connection types 1 and 2 have slots cut in the wall web plates to receive the coupling beam flange plates, which are wider than the wall thickness, t_{sc}. The beam flange plates are connected to the wall web plates using complete-joint-penetration (CJP) groove welding from the outside. The web plates of the wall and coupling beam are separate. The web plates of the coupling beam overlap the web plates of the wall and are fillet welded from the outside. The common details of connection types 1 and 2 are shown in Figure 3.

Continuity of the wall flange (closure) plate is the only difference between these two connections. In connection type 1, the wall flange (closure) plate is interrupted where the beam flanges enter the wall webs, leading to monolithic concrete in the wall and coupling beam [Figure 4(a)]. In connection type 2, the flange (closure) plate is continuous, as shown in Figure 4(b), leading to the concrete being interrupted between the walls and the coupling beam. Connection type 2 was conceptualized to study the importance, or lack thereof, of the continuity of the vertical flange (closure) plate of the wall through the depth of the coupling beam. The beam flange plate is first inserted into the slots; the wall flange closure plate is then inserted and welded on to the wall web and beam flange plates all four sides. The beam web plates are lapped to the wall web plates and welded at the end. Connection types 1 and 2 are recommended when the design thicknesses of the wall and the

coupling beam web plates are not close to each other—that is, there is more than a quarter-inch difference between them.

Connection types 3 and 4 have a continuous wall and beam web (same plate). As shown in Figure 5, connection type 3 has slots cut in the wall web plates to receive the coupling beam flange plates, which are wider than the wall thickness, t_{sc}. The beam flange plates are connected to the wall web plates using complete joint penetration (CJP) welding from the outside. In connection type 4, the flange plates of the coupling beam have the same width as the inside-to-inside thickness of the wall ($t_{sc} - 2t_p$), as shown in Figure 6. The coupling beam flange plates are placed inside the wall web plates at the connection and are connected to the wall web plates using CJP groove welding.

For both connection types, the wall flange (closure) plate is interrupted where the coupling beam connects to the wall, resulting in monolithic concrete in the wall and coupling beam. The beam flanges were connected to wall flange (closure) plates using fillet welding as shown in Figures 5 and 6. Connection types 3 and 4 are recommended when the design thicknesses for the wall and the coupling beam web plates have less than a quarter-inch difference between them. Instead of using separate web plates for the wall and beam, the wall web plate can be continued in the beam.

Design of Coupling Beam-to-C-PSW/CF Connections

Coupling beam-to-C-PSW/CF connections for the 8- and 12-story archetype structures (with planar walls) were designed according to ANSI/AISC 341-22, Section H8.8, and AISC Design Guide 38. The coupling beam-to-C-PSW/CF connection was designed to develop and transfer 1.2 times the expected flexural capacity $M_{p,exp}$ (and corresponding capacity-limited shear force) of the coupling beam. Forces in the beam elements were calculated, and a mechanism to transfer the forces to the wall elements was identified. The connections were then detailed to have a higher capacity than the required forces.

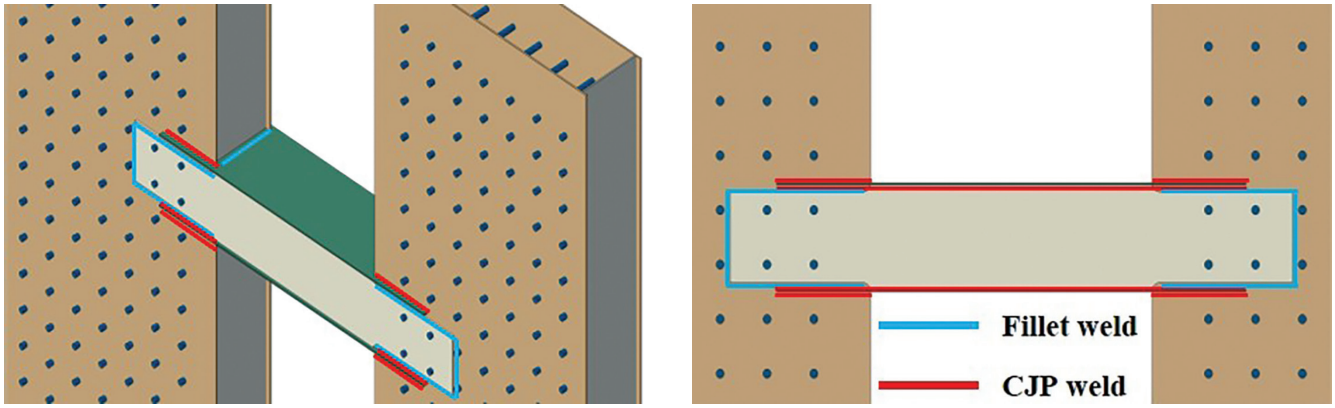

(a) Connection details *(b) Flange and web welding details*

Fig. 3. Common details of connection type 1 and 2.

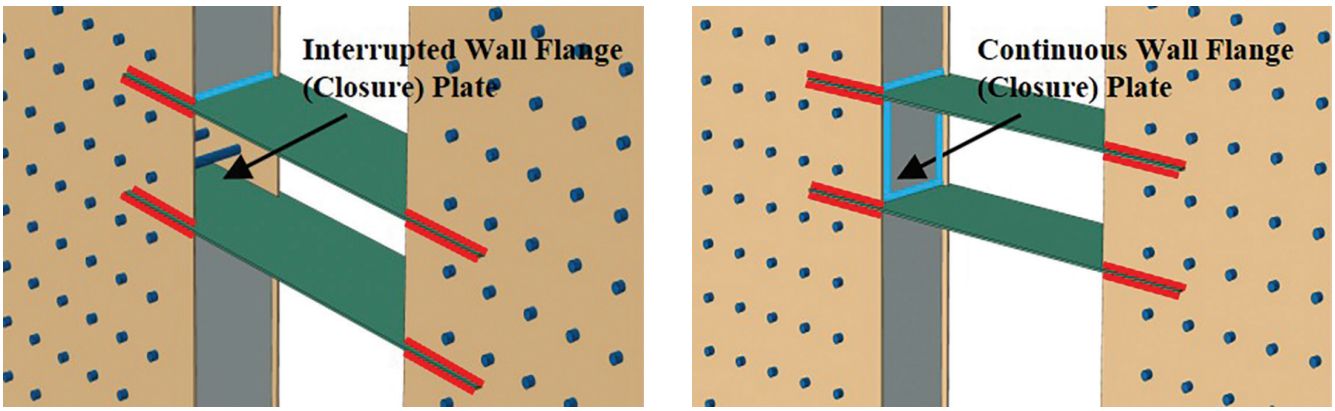

(a) Connection type 1 *(b) Connection type 2*

Fig. 4. Details of connection type 1 and type 2 (beam web plates are hidden).

The expected flexural capacity, $M_{p,exp}$, of the composite coupling beam was calculated using the plastic stress distribution method in the AISC *Specification for Structural Steel Buildings*, ANSI/AISC 360-22, Section I1.2 (AISC, 2022b), while using the expected yield strength, R_yF_y, for steel and the expected compressive strength, $R_cf'_c$, for concrete. Forces resisted by the flange plates, web plates, and concrete infill of the beam are transferred to the walls through the following connection elements:

1. Beam flange-to-wall web connection
2. Beam flange-to-wall flange connection
3. Beam web-to-wall web connection
4. Direct bearing of beam infill concrete to wall concrete

Preliminary finite element analyses of the coupling beam-to-C-PSW/CF connections showed the stresses in the beam flange were transferred to the wall primarily through the beam flange-to-wall web connection, which was also confirmed later by experimental results. The stress transfer through the beam flange-to-wall flange connection was negligible; therefore, the beam flange-to-wall web connection was designed to transfer the entire force in the beam flange, and the beam flange-to-wall flange connection was made using nominal fillet welds. The compression in the beam infill concrete was assumed to be transferred to the wall infill concrete through direct bearing. The required strength and available capacity calculation for the remaining two connection elements, beam flange-to-wall web and beam web-to-wall web, are discussed in the following sub-sections.

Coupling Beam Flange-to-Wall Web Connection

The coupling beam flange-to-wall web weld was designed to transfer the minimum of 120% of the expected tensile yield capacity and 100% of the expected tensile rupture

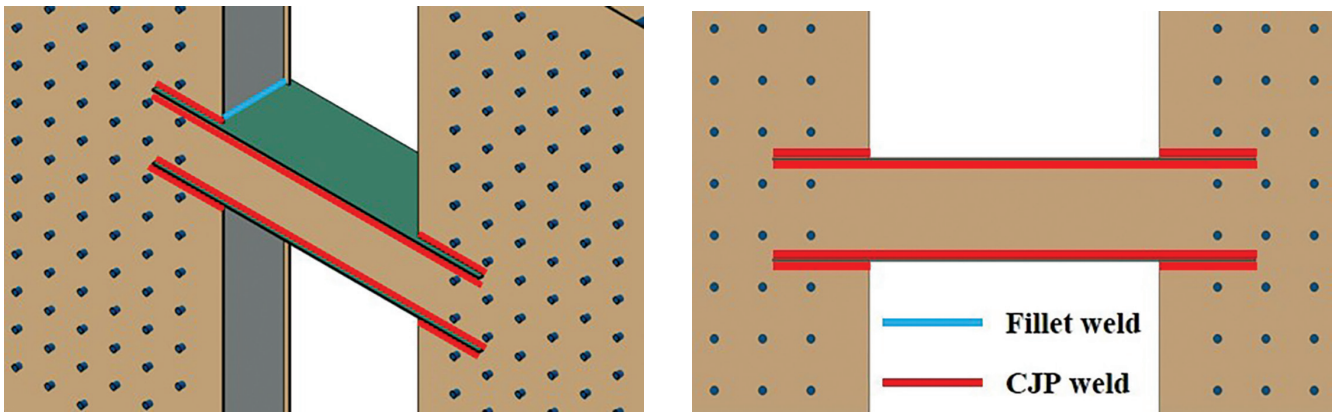

(a) Connection details *(b) Flange welding details*

Fig. 5. Details of connection type 3.

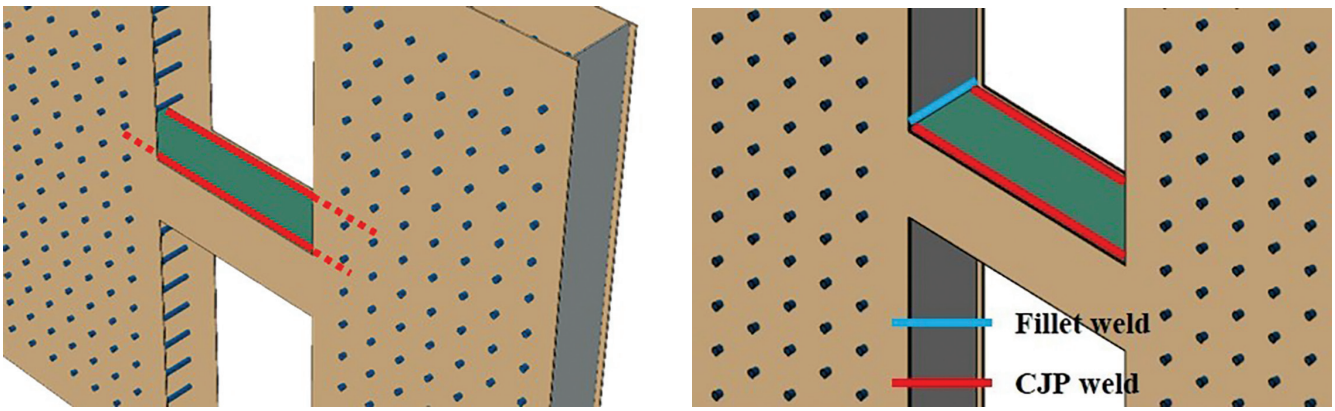

(a) Flange welding details *(b) Connection details*

Fig. 6. Details of connection type 4.

Table 2. Coupling Beam Flange-to-Wall Web Connection Calculations for Archetype Structures								
Case	**PG-1A**	**PG-1B**	**PG-1C**	**PG-2B**	**PG-1D**	**PG-1E**	**PG-1F**	**PG-2E**
Flange plate connection demand								
$1.2R_yF_yA_{f\_CB}$, kips	545	858	858	149	413	693	858	124
$R_tF_uA_{f\_CB}$, kips	590	930	930	161	447	751	930	134
T_{flange}, kips	545	858	858	149	413	693	858	124
Length of weld/flange embedment length								
L_{req}, in.	12.1	14.3	14.3	6.6	11	13.2	14.3	5.5
$L_{provided}$, in.	24	26	26	18	24	24	26	18
Shear strength of beam flange plates								
$\phi_d 0.6R_yF_yA_{f\_SY}$, kips	297	429	429	111	248	347	429	111
$\phi_n 0.6R_tF_uA_{f\_SR}$, kips	347	502	502	130	521	405	502	130
$\frac{T_{flange}}{2}$, kips	272	429	429	74	206	347	429	62
Shear strength of wall web plates								
$\phi_d 0.6R_yF_yA_{w\_SY}$, kips	891	965	1073	223	891	891	965	223
$\phi_n 0.6R_tF_uA_{w\_SR}$, kips	1042	1129	1255	261	1042	1042	1129	261
$\frac{T_{flange}}{2}$, kips	272	429	429	74	206	347	429	62

capacity of the flange plate, as shown in Equation 1. The length of the weld and the corresponding flange embedment length were estimated using Equation 2 to transfer this required tensile force from the beam flange to the wall web. Limit states of shear yielding and shear rupture of the beam flange and wall web plates at the connection were checked against the tension demand using Equations 3 to 6.

$$T_{flange} = \min\left(1.2R_yF_yA_{f\_CB}, R_tF_uA_{f\_CB}\right) \quad (1)$$

$$L_{req} \geq \frac{T_{flange}}{n\left(\phi_d 0.6F_y t_{p,f\_CB}\right)} \geq d \quad (2)$$

$$\frac{T_{flange}}{2} \leq \phi_d 0.6R_yF_yA_{f\_SY} \quad (3)$$

$$\frac{T_{flange}}{2} \leq \phi_n 0.6R_tF_uA_{f\_SR} \quad (4)$$

$$\frac{T_{flange}}{2} \leq \phi_d 0.6R_yF_yA_{w\_SY} \quad (5)$$

$$\frac{T_{flange}}{2} \leq \phi_n 0.6R_tF_uA_{w\_SR} \quad (6)$$

where

A_{f_CB} = cross-sectional area of the coupling beam flange, in.^{2}

A_{f_SR} = net shear area of coupling beam flange plate in shear rupture, in.^{2}

A_{f_SY} = gross shear area of coupling beam flange plate in shear yielding, in.^{2}

A_{w_SR} = net shear area of wall web plate in shear rupture, in.^{2}

A_{w_SY} = gross shear area of wall web plate in shear yielding, in.^{2}

n = number of weld lines connecting each end of beam flange to wall web; equal to 4 for connection types 1, 2, and 3, and equal to 2 for connection type 4

t_{p,f_CB} = thickness of coupling beam flange plate, in.

ϕ_d = 1.00

ϕ_n = 0.90

Sample beam flange-to-wall web connection calculations (with n equal to 4 for connection types 1, 2, and 3) for the archetype structures are presented in Table 2. The calculations are performed using F_y and F_u values of 50 and 65 ksi, respectively, considering an additional inch of overhang on each side of the beam flange to provide welding clearance, as shown in Figures 3, 4, and 5. Potential shear yielding and rupture planes for the coupling beam flange and wall web plates are shown in Figure 7 using yellow lines. Multiple yielding and rupture planes can be checked as applicable. Table 2 summarizes the limits for the cases presented here.

Coupling Beam Web-to-Wall Web Connection

For connection types 1 and 2, with separate beam and wall web plates, the beam web-to-wall web connection was designed to transfer the combination of capacity-limited shear, flexure, and axial force resisted by the beam web plates. Because the plastic neutral axis of the composite section does not coincide with the centroid of the section, the webs are subjected to a net tensile force (T_{web}), moment (M_{web}), and shear (V_{web}), estimated using the stress block shown in Figure 8. Each C-shaped fillet weld group (shown in Figure 9) was designed to transfer one-half of the total force carried by the beam webs—that is, $T_{c,weld}$, $M_{c,weld}$, and $V_{c,weld}$.

The C-shaped weld group connecting the beam web-to-wall web was designed for simultaneous flexure, shear, and tension as follows. AISC *Steel Construction Manual* (AISC, 2023) Table 8-8 was used to design the C-shaped weld group for the combination of flexure and shear, which were converted to an eccentric shear force producing an equivalent effect using Equation 7. This equivalent shear was applied to the C-shaped weld, as shown in Figure 9. The horizontal and vertical weld lengths of the C-shaped welds are also identified in Figure 9. Equations 8 to 12 were used to calculate the strength, $P_{weld,V}$, of the C-shaped weld group subjected to eccentric shear using AISC *Manual* Table 8-8. The strength of the weld group for resisting tension, $P_{weld,H}$, was estimated using Equation 13 in accordance with ANSI/AISC 360-22, Section J2.4, while considering only the horizontal welds of the C-shaped weld group. Finally, the utilization ratio for simultaneous tension and eccentric shear was estimated using the sum of the squared terms (SRSS) method and the individual demand-to-capacity ratios $\left(\frac{V_{c,weld}}{P_{weld,V}} \text{ and } \frac{T_{c,weld}}{P_{weld,H}}\right)$ as shown in Equation 14.

$$Eccentricity(Ecc) = \frac{M_{c,weld}}{V_{c,weld}} \tag{7}$$

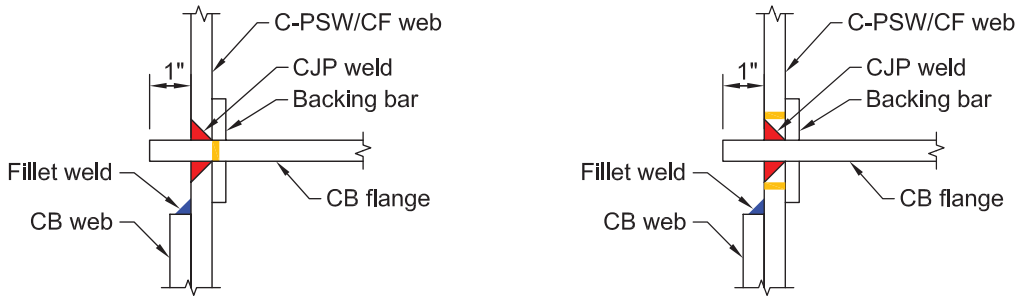

(a) CB flange shear yielding and rupture plane

(b) C-PSW/CF web shear yielding and rupture plane

Fig. 7. Possible shear yielding and rupture planes (shown using yellow lines).

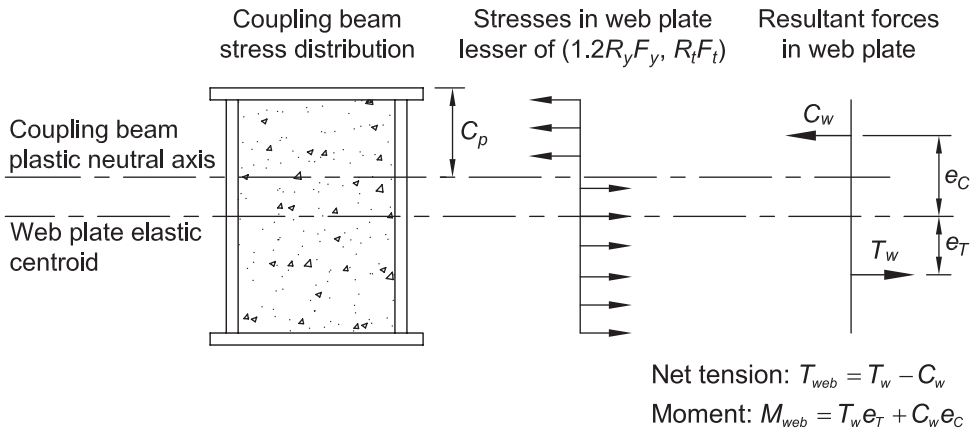

Fig. 8. Tension and moment in coupling beam web plates.

$$cg = \frac{2L_{web,H,weld}\,0.5L_{web,H,weld}}{2L_{web,H,weld}L_{web,V,weld}} \quad (8)$$

$$e_x = Ecc + L_{web,H,weld} - cg \quad (9)$$

$$k = \frac{L_{web,H,weld}}{L_{web,V,weld}} \quad (10)$$

$$a = \frac{e_x}{L_{web,V,weld}} \quad (11)$$

$$P_{weld,V} = \phi_n C_{8.8} C_1 (16w) L_{web,V,weld} \quad (12)$$

$$P_{weld,H} = \phi_n 0.6 F_{EXX}\, 2L_{web,H,weld}\,(0.707w) \quad (13)$$

$$\sqrt{\left(\frac{V_{c,weld}}{P_{weld,V}}\right)^2 + \left(\frac{T_{c,weld}}{P_{weld,H}}\right)^2} \le 1.0 \quad (14)$$

where

C_1 = electrode strength coefficient
$C_{8\cdot8}$ = coefficient tabulated in AISC *Manual* Table 8-8
F_{EXX} = filler metal classification strength, ksi
w = fillet weld size, in.

Sample beam web-to-wall web connection calculations for the archetype structures are presented in Table 3. It includes the forces resisted by the coupling beam web plates, the demands on the C-shaped welds, the weld geometry including fillet weld size w, the calculated eccentric shear strength, the tension strength, and the utilization ratio. The utilization ratio for all archetype structure connections was approximately 0.8, less than the maximum permissible limit of 1.0.

Detailed section and connection design calculations for an archetype structure (PG-1A) are included in Varma et al. (2021).

TEST SPECIMEN DETAILS

The test specimens designed and fabricated for this study were approximately one-half scale representations of the archetype structure connections. The scaling of the specimens was limited by the testing capacity available in the laboratory. A portion of the coupled system, including one-half of the coupling beam length and one composite wall, was selected to study the connection's response under cyclic lateral loading. The shear force and bending moment distribution in a coupling beam, with the inflection point located at the beam mid-span, was replicated using the half-beam cantilever subassembly. Gong and Shahrooz (2001) and Farsi et al. (2016) have used similar subassembly test setups in the past.

Test Matrix

The test specimens were not precisely scaled representations of any specific archetype structure; instead, they were designed to estimate the fundamental behavior under the constraints of the available laboratory capabilities. Two specimens of connection types 1 and 2 and one specimen of connection types 3 and 4, with beam clear span-to-section depth ratios, L_b/d, of 3.5 and 5.1, were selected as shown in the final test matrix in Table 4. It includes the specimen designation, connection type, and the L_b/d ratio. Geometric details of the wall and coupling beam are given in Table 4 and shown in Figure 10, including:

Wall:

H_w = height, in.
L_w = length, in.
t_{f_w} = flange thickness, in.
t_{sc} = thickness, in.
t_{w_w} = web thickness, in.

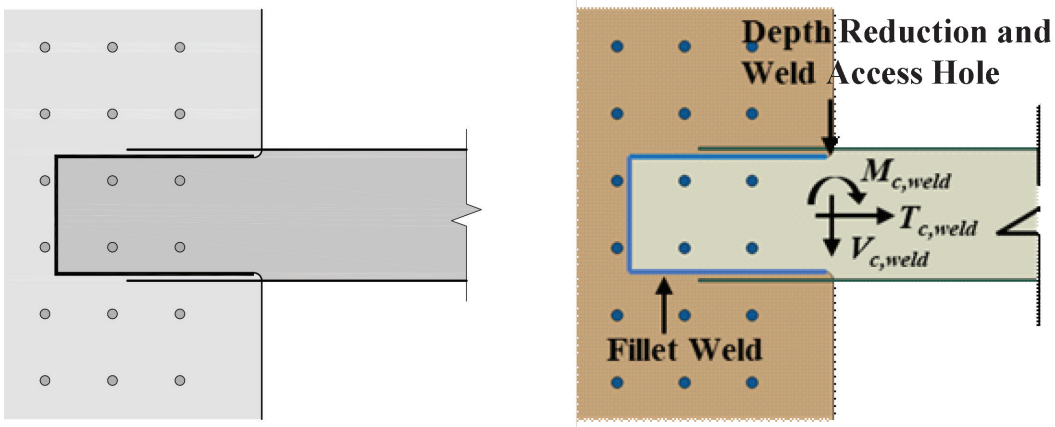

Fig. 9. C-shaped fillet weld connecting beam web-to-wall web.

Table 3. Coupling Beam Web-to-Wall Web Connection Calculations for Archetype Structures								
Case	**PG-1A**	**PG-1B**	**PG-1C**	**PG-2B**	**PG-1D**	**PG-1E**	**PG-1F**	**PG-2E**
Forces in beam web plates								
T_{web}, kips	738	778	778	331	712	759	778	297
M_{web}, kip-in.	3941	3491	3491	1732	4202	3706	3491	1895
V_{web}, kips	662	650	520	185	575	570	520	169
Force demand on C-shaped weld								
$T_{c,weld}$, kips	369	389	389	166	356	380	389	149
$M_{c,weld}$, kip-in.	1971	1746	1746	866	2101	1853	1746	948
$V_{c,\ weld}$, kips	331	325	260	93	288	285	260	85
Weld geometry								
$L_{web,V,weld}$, in.	22	22	22	16	22	22	22	16
$L_{web,H,weld}$, in.	44	44	44	20	44	44	44	20
w, in.	5⁄16	5⁄16	5⁄16	¼	5⁄16	5⁄16	5⁄16	¼
C-shaped weld eccentric shear capacity								
Ecc, in.	5.95	5.38	6.72	9.36	7.31	6.51	6.72	11.2
cg, in.	17.6	17.6	17.6	7.14	17.6	17.6	17.6	7.14
e_x, in.	32.4	31.8	33.1	22.2	33.7	32.9	33.1	24.1
k	2.00	2.00	2.00	1.25	2.00	2.00	2.00	1.25
a	1.47	1.44	1.51	1.39	1.53	1.50	1.51	1.51
$C_{8.8}$	4.97	5.04	4.90	2.93	4.81	4.91	4.88	2.74
$P_{weld,V}$, kips	492	499	485	169	477	486	483	158
C-shaped weld tension capacity								
$P_{weld,H}$, kips	735	735	735	267	735	735	735	267
Utilization of weld capacity								
$\frac{V_{c,weld}}{P_{weld,V}}$	0.67	0.65	0.54	0.55	0.60	0.59	0.54	0.53
$\frac{T_{c,weld}}{P_{weld,H}}$	0.50	0.53	0.53	0.62	0.48	0.52	0.53	0.56
Utilization ratio	0.84	0.84	0.75	0.83	0.77	0.78	0.75	0.77

Table 4. Details of Composite Coupling Beam-to-C-PSW/CF Connection Specimens												
Specimen	**Connection Type**	**L_b/d Ratio**	**Coupling Beam Dimensions, in.**					**Wall Dimensions, in.**				
			b_f	**b_i**	**d**	**t_{f_b}**	**t_{w_b}**	**t_{sc}**	**t_{f_w}**	**t_{w_w}**	**H_w**	**L_w**
SP-1	1	5.1	12.875	11.5	12.5	¼	3⁄16	11.5	¼	¼	120	38.5
SP-2	2	5.1	12.875	11.5	12.5	¼	3⁄16	11.5	¼	¼	120	38.5
SP-3	1	3.5	13.25	11.5	12.5	¼	⅜	11.5	¼	¼	120	29.25
SP-4	2	3.5	13.25	11.5	12.5	¼	⅜	11.5	¼	¼	120	29.25
SP-5	3	3.5	12.5	10.75	12.5	¼	⅜	11.5	¼	⅜	120	29.25
SP-6	4	3.5	10.75	10.75	12.5	¼	⅜	11.5	¼	⅜	120	29.25

Coupling beam:

b_f = flange width, in.
b_i = inside-to-inside distance between webs, in.
d =total depth of cross section, in.
t_{f_b} = flange thickness, in.
t_{w_b} = web thickness, in

Specimens SP-1 (connection type 1) and SP-2 (connection type 2), with an approximately square cross section and L_b/d ratio of 5.1, represent the thicker wall web and thinner beam web plate design of archetypes PG-1C and PG-1F. Specimens SP-3 (connection type 1) and SP-4 (connection type 2) represent the thinner wall web and thicker beam web plate design of archetypes PG-2B and PG-2E, but with an approximately square cross section of the beam and an L_b/d ratio of 3.5. Specimens SP-5 (connection type 3) and SP-6 (connection type 4), with L_b/d ratio of 3.5 are representative of archetypes PG-1A and PG-1D, but with an approximately square cross section of the beam and web plate that is of equal thickness and continuous for both the coupling beam and the composite wall. Fabrication drawings of all six specimens are presented in Figures 11 and 12.

Design of Test Specimens

The C-PSW/CF, coupling beam, and the connection between the two members were designed following the requirements in ANSI/AISC 360-22 and ANSI/AISC 341-22, which are also described in detail in AISC Design Guide 38.

Design of C-PSW/CF

The steel plates were designed to comprise between 1% and 10% of the total composite cross section, as specified in ANSI/AISC 360-22, Section I1.6. The opposite web plates were connected using tie bars, and the tie bars and stud anchors also anchored the plates to the concrete infill. In accordance with ANSI/AISC 341-22, Section H7.5a, the steel plates must be nonslender—that is, yielding in compression occurs before local buckling, which can be achieved using Equation 15.

$$\frac{b}{t_p} \le 1.05\sqrt{\frac{E_s}{R_y F_y}} \tag{15}$$

where

b = largest unsupported length of the plate between rows of steel anchors or ties, in.
t_p = steel plate thickness of C-PSW/CF wall webs, identified as t_{w_w} in Figure 10, in.

The maximum allowable tie bar spacing is limited to 1.0 times the wall thickness, t_{sc}, per ANSI/AISC 360-22, Section I1.6b. Additionally, the detailing of the empty steel modules (before concrete casting) in terms of the maximum slenderness ratio for the steel plates (S/t_p) and the tie bar diameter and spacing are limited to provide adequate shear stiffness and stability using Equation 16, developed by Varma et al. (2019), and required by ANSI/AISC 360-22, Section I1.6b.

$$\frac{S}{t_p} \le 1.0\sqrt{\frac{E_s}{2\alpha + 1}} \tag{16}$$

$$\alpha = 1.7\left(\frac{t_{sc}}{t_p} - 2\right)\left(\frac{t_p}{d_{tie}}\right)^4 \tag{17}$$

where

S = largest clear spacing of the ties, in.
d_{tie} = effective diameter of the tie, in.

Tie bars of low carbon ASTM A1018/A1018M steel, with ½ in. diameter, were uniformly spaced at 6 in. in both directions. They were welded to the wall web plates using 5⁄16 in. fillet welds around the circumference of the bar on the outside of wall web plates to develop the full yield strength of the tie bar. Table 5 shows the section details of the wall to be within limits prescribed by the design code.

Design of Composite Coupling Beam

The cross-section areas of the steel elements were designed to be greater than 1% of the total composite cross section, per ANSI/AISC 360-22, Section I2.2a. The section was

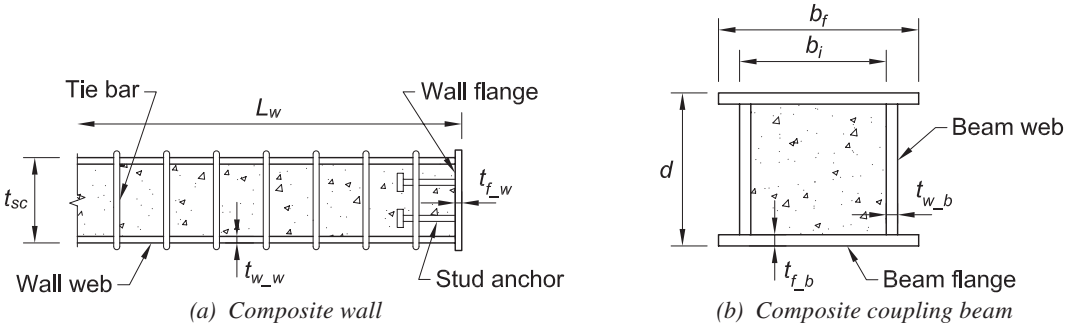

(a) Composite wall *(b) Composite coupling beam*

Fig. 10. Cross-section details of specimens.

Table 5. Section Details of C-PSW/CF						
Specimen	Percentage of Steel	$\frac{b}{t_p}$	$1.05\sqrt{\frac{E_s}{R_yF_y}}$	$\frac{S}{t_p}$	α	$1.0\sqrt{\frac{E_s}{2\alpha+1}}$
SP-1	4.7%	24.0	24.3	24.0	4.70	52.9
SP-2	4.7%	24.0	24.3	24.0	4.70	52.9
SP-3	4.7%	24.0	24.3	24.0	4.70	52.9
SP-4	4.7%	24.0	24.3	24.0	4.70	52.9
SP-5	6.9%	16.0	24.3	16.0	15.4	30.2
SP-6	6.9%	16.0	24.3	16.0	15.4	30.2

Table 6. Section Details of Composite Coupling Beams									
Specimen	Percentage of Steel	$\frac{b_c}{t_{f\_b}}$	$2.37\sqrt{\frac{E_s}{R_yF_y}}$	$\frac{h_c}{t_{w\_b}}$	$2.66\sqrt{\frac{E_s}{R_yF_y}}$	L_b, in.	$M_{p,exp}$, kip-in.	$\frac{1.2(2M_{p,exp})}{L_b}$, kips	$V_{n,exp}$, kips
SP-1	7.4%	46.0	54.9	64*	61.6	31.25	3290	126	156
SP-2	7.4%	46.0	54.9	64*	61.6	31.25	3290	126	156
SP-3	10.2%	46.0	54.9	32	61.6	21.0	4262	244	313
SP-4	10.2%	46.0	54.9	32	61.6	21.0	4262	244	313
SP-5	10.6%	43.0	54.9	32	61.6	21.0	4034	231	307
SP-6	10.7%	43.0	54.9	32	61.6	21.0	3687	211	322

* The ratio of $\frac{h_c}{t_{w\_b}}$ is slightly higher than the slenderness limit, but it was deemed to be adequate for these tests.

designed to be compact with slenderness ratios of flanges and webs limited per Equations 18 and 19 in accordance with ANSI/AISC 341-22, Section H8. The web slenderness requirement is established to develop the shear yield strength before shear buckling. The flange slenderness requirement is established to develop the compression yield strength before elastic buckling.

$$\frac{b_c}{t_{f\_b}} \le 2.37\sqrt{\frac{E_s}{R_yF_y}} \tag{18}$$

$$\frac{h_c}{t_{w\_b}} \le 2.66\sqrt{\frac{E_s}{R_yF_y}} \tag{19}$$

where

b_c = clear unsupported width of the coupling beam flange plate, in.

h_c = clear unsupported width of the coupling beam web plate, in.

The section was proportioned to be flexure-critical by designing the shear strength to be greater than the capacity-limited shear due to the expected flexural capacity, as shown in Equation 20, which is in accordance with ANSI/AISC 341-22, Section H8.8. The capacity-limited shear force is increased by 1.2 to account for steel inelastic hardening, concrete confinement, and the biaxial (tensile) stress state in the steel tension flange.

Table 6 shows the structural characteristics of the composite coupling beams to be within the limits prescribed by ANSI/AISC 341-22, Section H8.

$$V_{n,exp} \ge \frac{1.2(2M_{p,exp})}{L_b} \tag{20}$$

where

L_b = clear span length of the coupling beam, in.

$M_{p,exp}$ = expected flexural capacity of composite coupling beam calculated using the plastic stress distribution method specified in ANSI/AISC 360-22, Section I1.2, while using the expected yield strength for steel, R_yF_y, and the expected compressive strength, R_cf_c', for concrete, kip-in.

$V_{n,exp}$ = expected shear strength of composite coupling beam calculated per ANSI/AISC 360-22, Section I4.2, while using expected yield strength, R_yF_y, for steel, and expected compressive strength, R_cf_c', for concrete, kips

Table 7. Coupling Beam Flange-to-Wall Web Connection Calculations for CC-PSW/CF Specimens				
Case	**SP-1, SP-2**	**SP-3, SP-4**	**SP-5**	**SP-6**
Flange plate connection demand				
$1.2R_yF_yA_{f\_CB}$, kips	209	215	203	174
$R_tF_uA_{f\_CB}$, kips	232	239	225	194
T_{flange}, kips	209	215	203	174
Length of weld/flange embedment length				
L_{req}, in.	10.75	10.0	9.4	16.1**
$L_{provided}$, in.	12.5	12.5	12.5	12.5
Shear strength of beam flange plates				
$\phi_d 0.6R_yF_yA_{f\_SY}$, kips	101***	101***	101	101
$\phi_n 0.6R_tF_uA_{f\_SR}$, kips	122	122	122	122
$\frac{T_{flange}}{2}$, kips	104	107	101	87
Shear strength of wall web plates				
$\phi_d 0.6R_yF_yA_{w\_SY}$, kips	203	203	304	304
$\phi_n 0.6R_tF_uA_{w\_SR}$, kips	243	243	365	182
$\frac{T_{flange}}{2}$, kips	104	107	101	87

** Designed for F_y = 50 ksi, but the calculations are presented for 36 ksi. The length of weld provided (equal to 1.0*d*) satisfies the requirement for minimum length when calculated using the measured F_y of 48 ksi. The calculation should be performed for a range of yield strengths for an actual structure. The plates procured should be required to have measured yield strength within the checked limits to ensure that the beam and wall elements yield in sequence, as intended during the design process.

*** The shear yield strength of the coupling beam flange plates is lower but close to the value required to transfer half the tension in the flange, thus the length of weld provided (equal to 1.0*d*) was deemed to be adequate.

Design of Connections

Connections at the section level and at the member level were designed for the specimens. At the section level, tie bar-to-steel plate connections, coupling beam flange-to-web connections, and wall flange-to-web connections were sized. The tie bars-to-steel plate connection was designed to develop the yield strength of the bar in tension, using 5⁄16 in. welds going around the bar's circumference on the outside of wall web plates. The flange-to-web connections in the beam and wall were designed to develop the expected yield strength of the weaker base metal plate. Flange-to-web connections in the wall utilized ¼ in. fillet welds. For flange-to-web welds in the beam, complete joint penetration groove welds were used for the specimens with an L_b/d ratio of 3.5 and ¼ in. fillet welds for specimens with an L_b/d ratio of 5.1. Although the connection was required to develop the full yield strength of the base metal, the specimens were smaller-scaled versions of the archetypes, and the thin 3⁄16 in. plate would distort excessively due to the heat from groove welding. Consequently, fillet welds were adopted as they fused through the thickness of 3⁄16 in. plates and effectively provided complete joint penetration. The coupling beam-to-C-PSW/CF connections were designed at the member level using methods presented earlier in the design of connections for archetype structures.

Coupling Beam Flange-to-Wall Web Connection

For specimens with L_b/d ratio of 3.5 (SP-3, SP-4, SP-5, SP-6), prequalified CJP weld configuration TC-U4a-GF was used to connect the beam flange to the wall web. The wider flange plate going inside the slots in wall web (SP-3, SP-4, and SP-5) was welded on two sides, as shown in Figures 3 and 5. The narrow flange plate fitted inside the wall thickness (SP-6) was welded on one side, as shown in Figure 6. The backing bars were left in place. Fillet welds were used for specimens with an L_b/d ratio of 5.1 (SP-1, SP-2). Sample calculations for the specimen beam flange-to-wall web connections are presented in Table 7. The calculations were performed using F_y and F_u values of 36 and 60 ksi, respectively. For specimens with a wider flange plate, half-an-in. of overhang was considered on each side of the beam flange to provide clearance for welding. Potential shear yielding and rupture planes for the coupling beam flange and wall web plates for connection types 1 and 2

Table 8. Coupling Beam Web-to-Wall Web Connection Calculations for CC-PSW/CF Specimens		
Case	**SP-1, SP-2**	**SP-3, SP-4**
Forces in beam web plates		
T_{web}, kips	200	304
M_{web}, kip-in.	465	1275
V_{web}, kips	129	252
Force demand on C-shaped weld		
$T_{c,\ weld}$, kips	100	152
$M_{c,\ weld}$, kip-in.	233	637.5
$V_{c,\ weld}$, kips	65	126
Weld geometry		
$L_{web,V,weld}$, in.	18.0	20.0
$L_{web,H,weld}$, in.	10.0	10.0
w, in.	3/16	5/16
C-shaped weld shear and moment capacity		
Ecc, in.	3.60	5.06
cg, in.	7.04	8.00
e_x, in.	14.56	17.06
k	1.80	2.00
a	1.46	1.71
$C_{8.8}$	4.21	4.41
$P_{weld,V}$, kips	114	198
C-shaped weld tension capacity		
$P_{weld,H}$, kips	180	334
Utilization of weld capacity		
$\frac{V_{c,weld}}{P_{weld,V}}$	0.57	0.64
$\frac{T_{c,weld}}{P_{weld,H}}$	0.55	0.46
Utilization ratio	0.79	0.78

are shown in Figure 7. Multiple yielding and rupture planes can be checked; Table 7 summarizes the limits for the cases presented.

Coupling Beam Web-to-Wall Web Connection

The coupling beam web-to-wall web connections were designed for Specimens SP-1, SP-2, SP-3, and SP-4 in accordance with Figures 8 and 9 and Equations 7 to 14, which were described earlier for the archetype structure connection design. All the corresponding calculations for Specimens SP-1 and SP-2 with length-to-depth ratio of 5.1 and Specimens SP-3 and SP-4 with length-to-depth ratio of 3.5 are provided in Table 8 along with the designed weld geometry. For Specimens SP-5 and SP-6, the coupling beam webs and wall webs were one continuous plate.

Fabrication Drawings

Figure 11 shows the elevation, section views, and weld details of specimens SP-1 and SP-3 (connection type 1) and specimens SP-2 and SP-4 (connection type 2). Figure 12 presents the same for specimens SP-5 (connection type 3) and SP-6 (connection type 4). The embedment length for the coupling beam flange and the lap length for the coupling beam web is also identified. The flange embedment

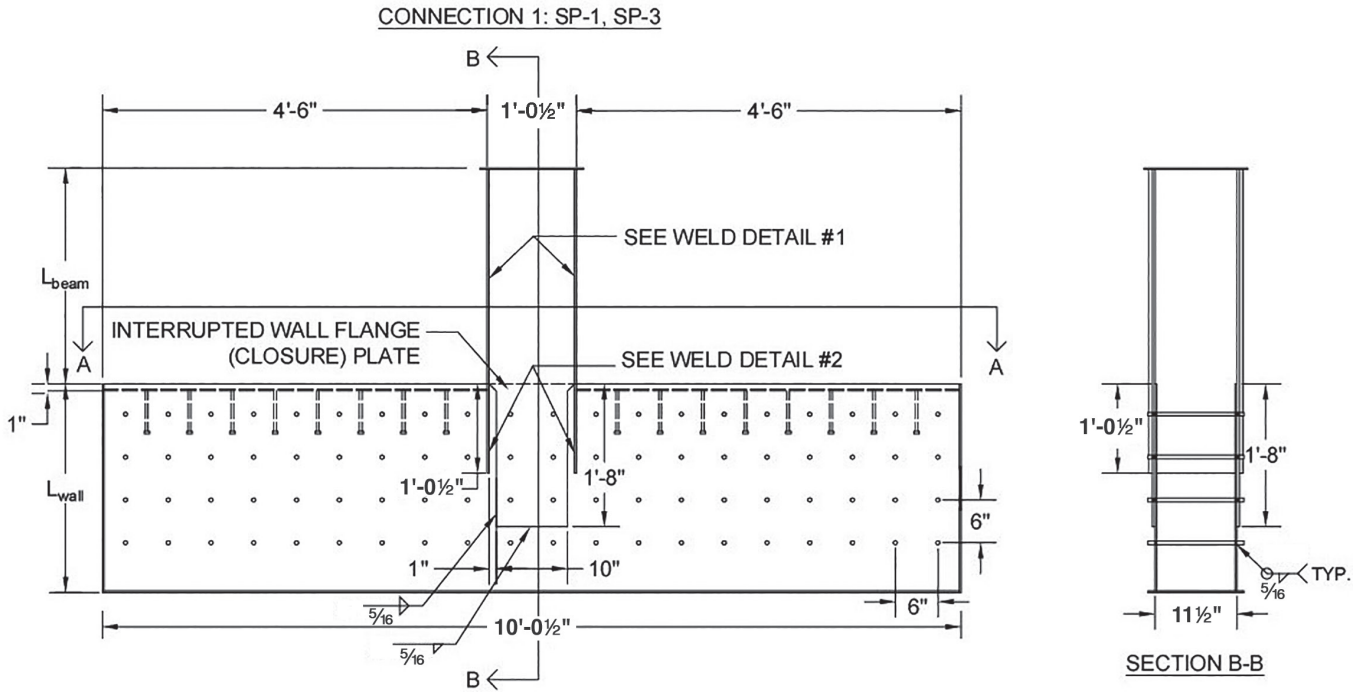

(a) Specimens SP-1 and SP-3

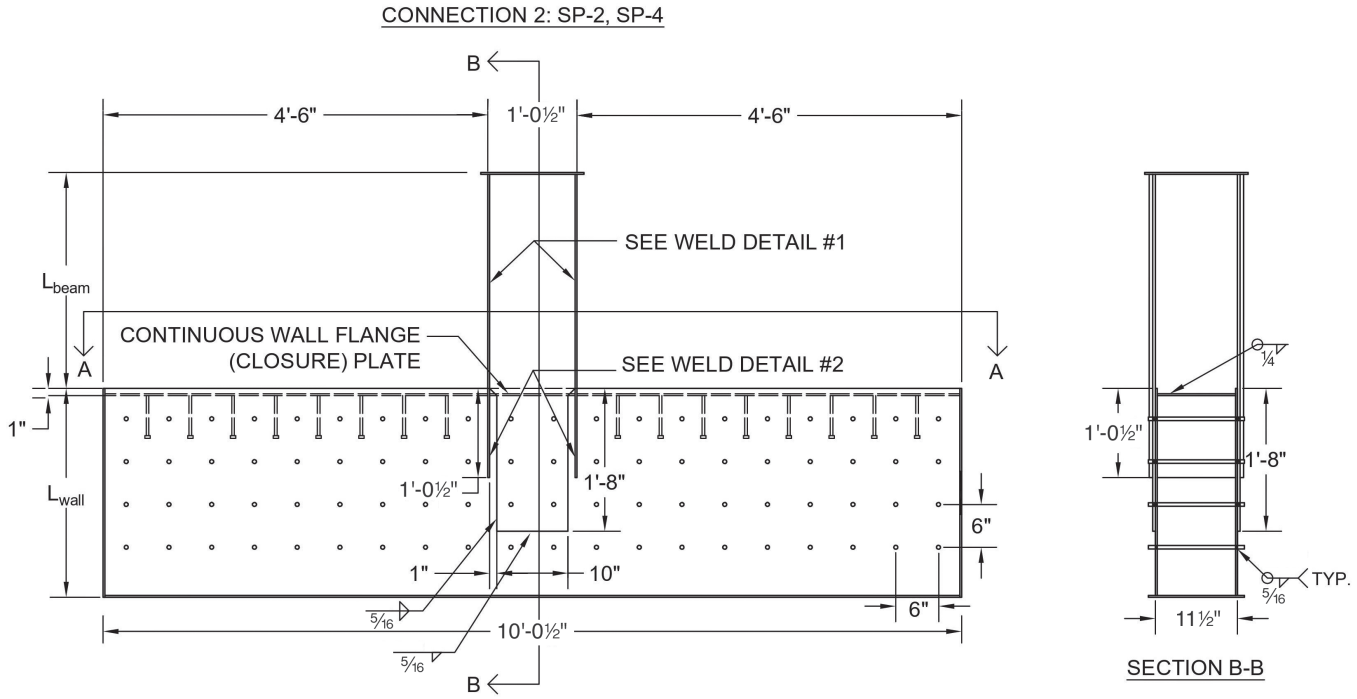

(b) Specimens SP-2 and SP-4

Fig. 11. Fabrication drawings—elevation and side view of specimens.

length was equal to the beam depth (d = 12.5 in.) for all connection types. A beam web-to-wall web lap length of 20 in. was provided for specimens with separate web plates for the beam and wall. The weld details and top section view for the connection are also shown in Figures 11 and 12.

For all connection types, specimens with an L_b/d ratio of 3.5 (SP-3, SP-4, SP-5, and SP-6) utilized prequalified CJP weld configuration TC-U4a-GF for the beam flange-to-beam web and beam flange-to-wall web connection. After welding, the backing bars were left in place. For specimens with L_b/d ratio of 5.1 (SP-1, SP-2), fillet welds were used for the beam flange-to-beam web and beam flange-to-wall web connections. The wall web was cut to receive the coupling beam flange plates at four locations. The plates making up the wall panel were connected using nominal ¼ in. fillet welds as the stresses away from the connection region were expected to be minimal.

TEST SETUP

Figure 13 shows a schematic of the test setup used for conducting the coupling beam-to-wall connection experiments. The composite wall was post-tensioned to the laboratory strong floor using high-strength post-tensioning bars. The

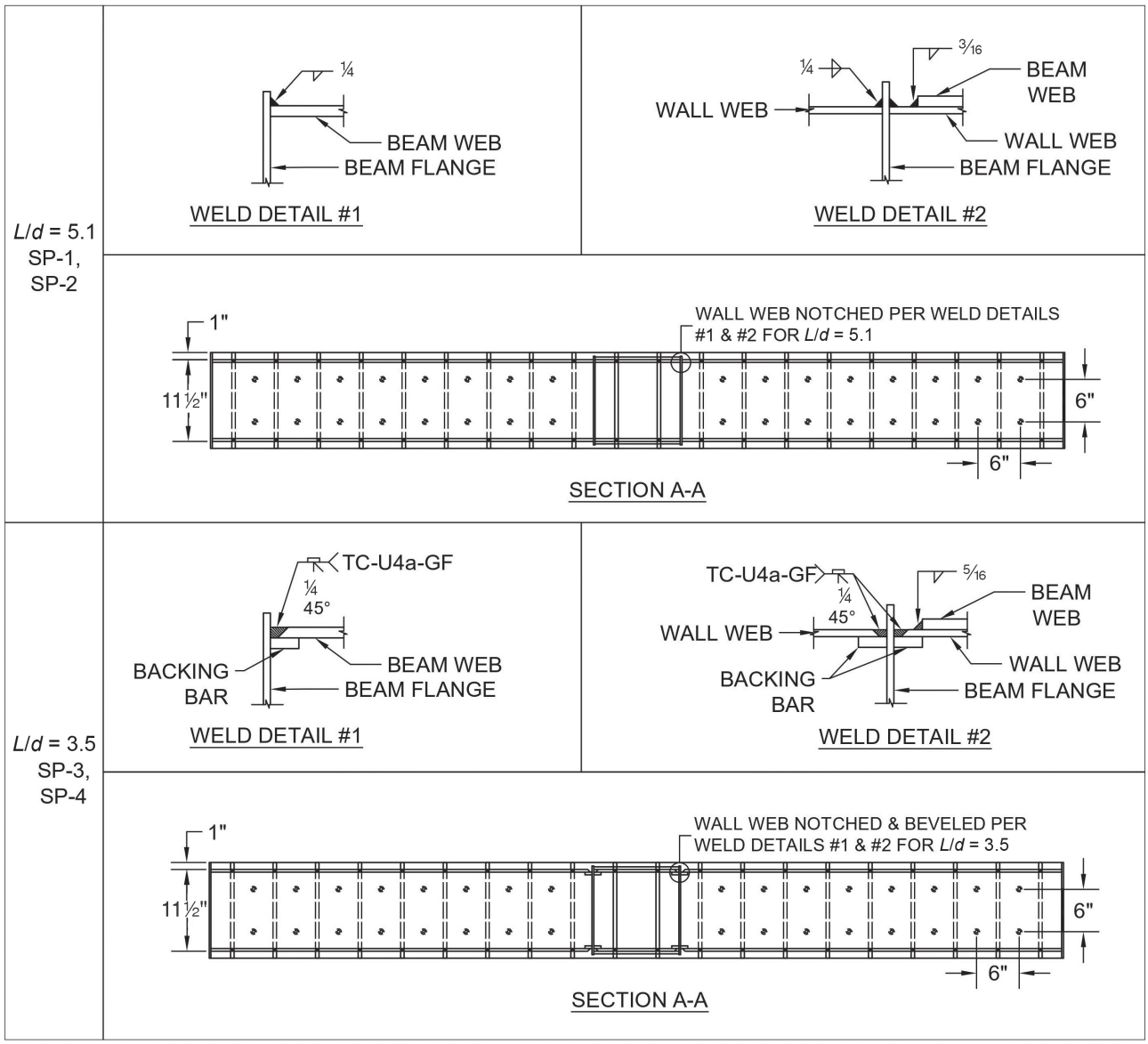

(c) Top view and connection details

Fig. 11. Fabrication drawings—elevation and side view of specimens (continued).

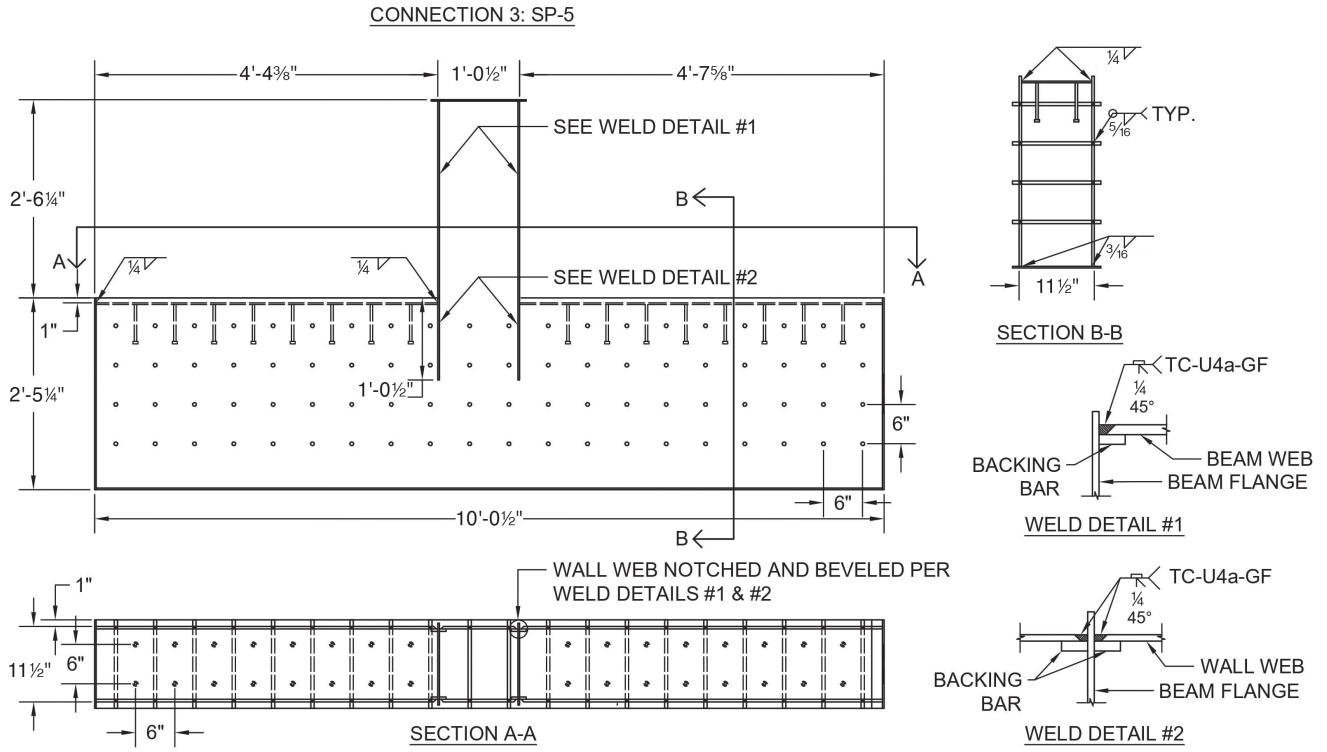

(a) Specimen SP-5

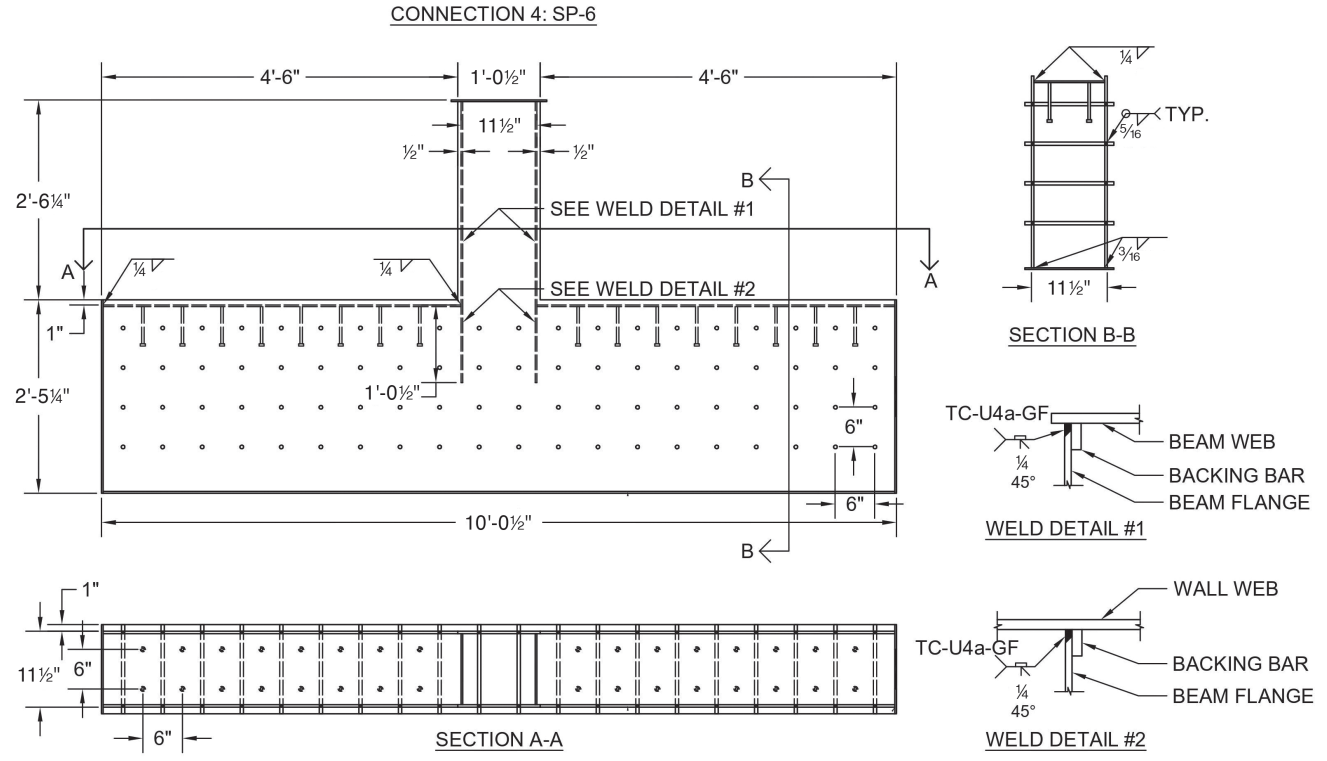

(b) Specimen SP-6

Fig. 12. Elevation, side, top views, and connection details of specimens.

coupling beam end was subjected to quasi-static lateral cyclic loading in accordance with the ATC-24 single specimen loading protocol (ATC, 1992). The lateral load was applied at the height of 31.875 in. or 21.75 in. from the top of the wall flange (closure) plate, thus achieving an L_b/d ratio of 5.1 or 3.5, respectively. Details of the experimental test setup are not presented here for brevity. They are presented in detail in Varma et al. (2021).

EXPERIMENTAL RESULTS AND OBSERVATIONS

Cyclic Response of Composite Coupling Beam-to-C-PSW/CF Connection

This section briefly presents the experimental behavior of one coupling beam-to-C-PSW/CF connection specimen (Specimen SP-1, connection type 1). The cyclic normalized moment-chord rotation response of specimen SP1 is shown in Figure 14. The moment, M, was calculated at the base of the coupling beam and normalized with respect to the nominal plastic moment capacity, M_p, of the coupling beam calculated using measured material properties and dimensions. Chord rotation, θ, was estimated by dividing the lateral displacement, Δ, at the point of load application by h, which is the coupling beam length between its base and the center point of load application. The figure includes (1) horizontal dashed lines corresponding to 80% of the nominal plastic moment capacity, M_p, and (2) vertical dashed lines corresponding to 0.03 rad chord rotation. Strain gauge data showed that all inelasticity occurred in the coupling beam flange and web, in the plastic hinge region that formed next to the connection region, and in the wall remained essentially elastic until the end of the test.

The behavior of specimen SP-1 was as follows according to the experimental observations and measurements. The cyclic lateral load-displacement response was approximately linear during the elastic cycles. The coupling beam infill concrete cracked in tension during the first elastic cycle, at a lateral force corresponding to 14% of the flexural capacity, M_p. Strain gauge data showed yielding of the beam flange and web plates in tension during the $1.0\Delta_y$ and $1.5\Delta_y$ cycles, respectively. Δ_y is defined as the peak displacement of the first inelastic cycle, projected from the displacement corresponding to the maximum elastic force level. Yielding was also confirmed by the flaking of whitewash applied to

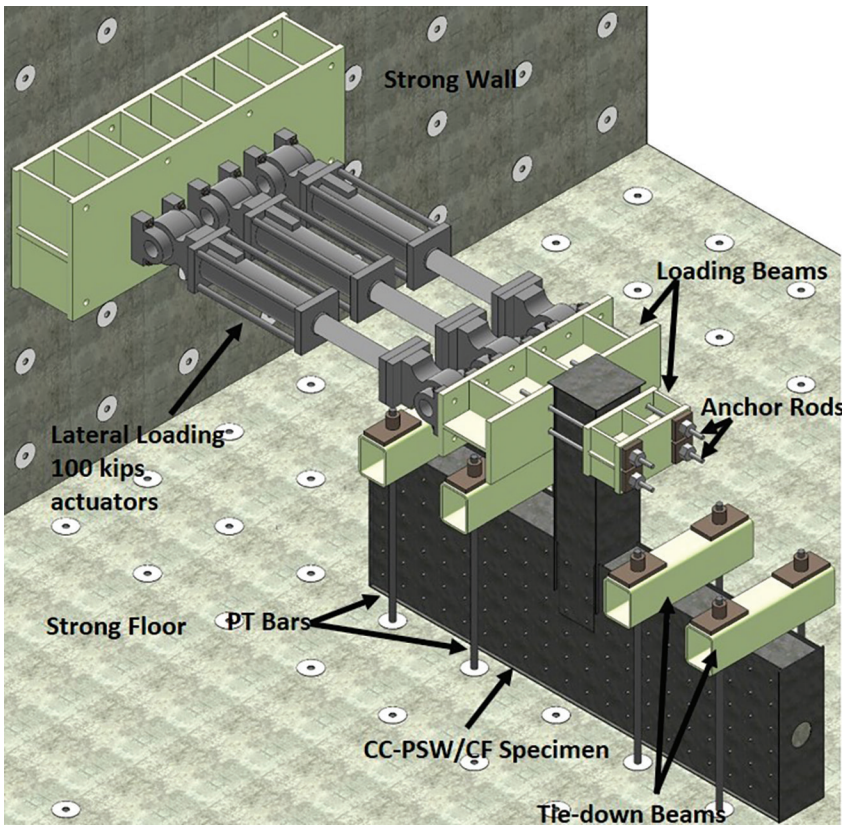

Fig. 13. Schematic view of the test setup.

the surface of steel plates in the connection region. Local buckling of compression flange was visually observed during the $2\Delta_y$ cycles, which was also confirmed by strain gauge results. The maximum flexural capacity was reached during the $2\Delta_y$ cycles. Steel fracture initiated in the base metal of the beam flange-to-wall web and the beam web-to-wall web welded connections during the 1 to $2\Delta_y$ cycles. The fracture propagated further in the beam flange and web plates during the $3\Delta_y$ cycles, which resulted in reduction of lateral load resistance in subsequent cycles. Extensive local bucking of flanges occurred during the 3, 4, and $5\Delta_y$ cycles. The beam flanges completely fractured under tension during the $5\Delta_y$ cycles.

Figure 15 shows the condition of connection at the end of the test. The whitewash was removed to get clear photographs of fracture at the end of the test. As shown in Figure 14, the average flexural capacity of the connection at chord rotation of 0.03 rad was higher than $0.8M_p$. The connection was thus deemed to satisfy the requirement of at least 0.03 chord rotation at 80% of the nominal plastic moment capacity M_p, specified by ANSI/AISC 341-22.

Comparison of Moment-Rotation Response for All Specimens

Figures 16(a)–16(e) present the cyclic, normalized moment-chord rotation responses of the remaining five specimens. These figures include horizontal lines corresponding to 80% of the nominal plastic moment capacity, M_p, calculated using plastic stress distribution method and vertical lines corresponding to the chord rotation of 0.03 rad. For each specimen, the envelopes of cyclic moment-rotation (M-θ) responses in each direction (push and pull) were developed and averaged. The backbone curve was developed by selecting the peaks of the first cycle at each force/displacement level. The push and pull curves comprised of the discrete peak points were then averaged. Figure 16(f) shows (and compares) these averaged normalized backbone moment-rotation (M-θ) curves for all specimens. As shown, the experimental capacities of all specimens exceeded the flexural capacities calculated using the plastic stress distribution method and measured material properties. All the coupling beam-to-C-PSW/CF connections developed chord-rotation capacities greater than 0.03 rad before the flexural strength degraded below 80% of M_p. The flexural capacities of the specimens were between 1.05 and 1.40 times the plastic flexural capacities of the composite coupling beams calculated using measured material properties.

CONCLUSIONS

Four different types of composite coupling beam-to-C-PSW/CF connections were developed and proposed

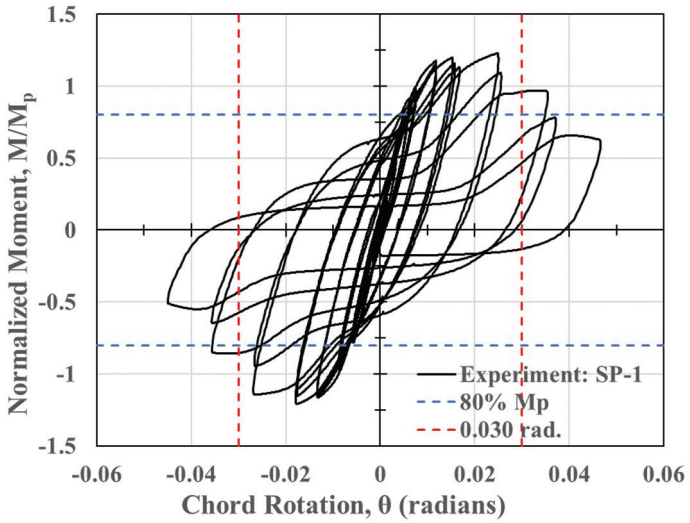

Fig. 14. Normalized moment—chord rotation curve of specimen SP-1 (connection type 1).

(a) North flange

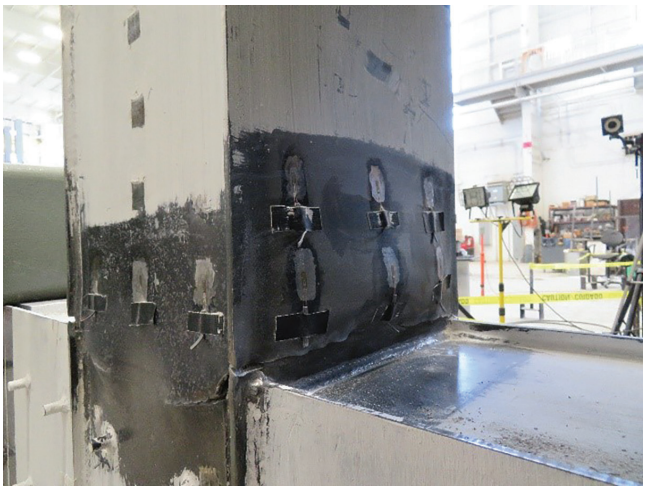

(b) South flange

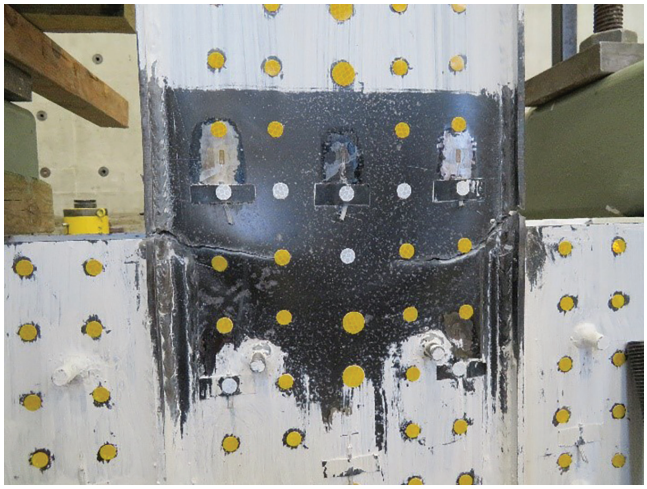

(c) East web

(d) West web

Fig. 15. End of test of SP-1 showing local buckling and fracture.

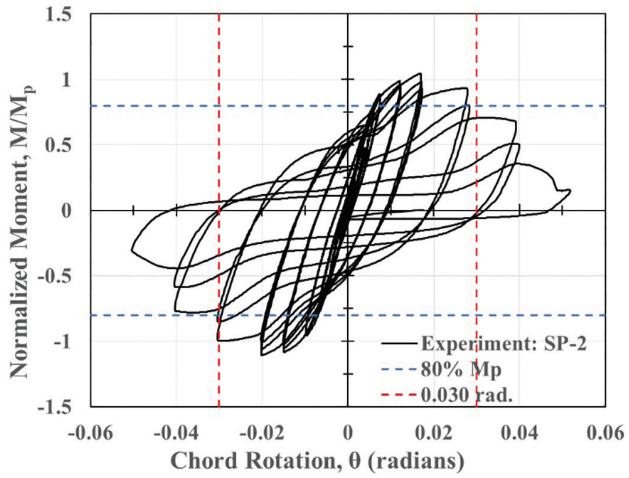

(a) Specimen SP-2

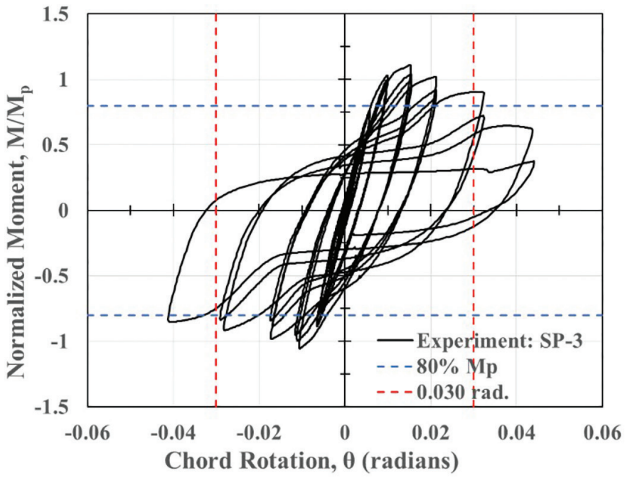

(b) Specimen SP-3

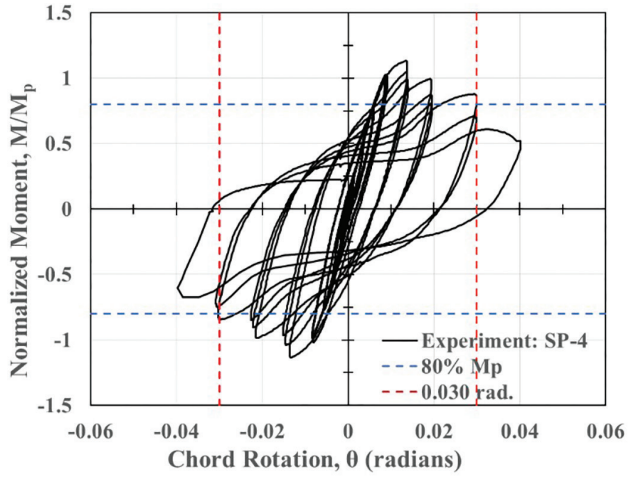

(c) Specimen SP-4

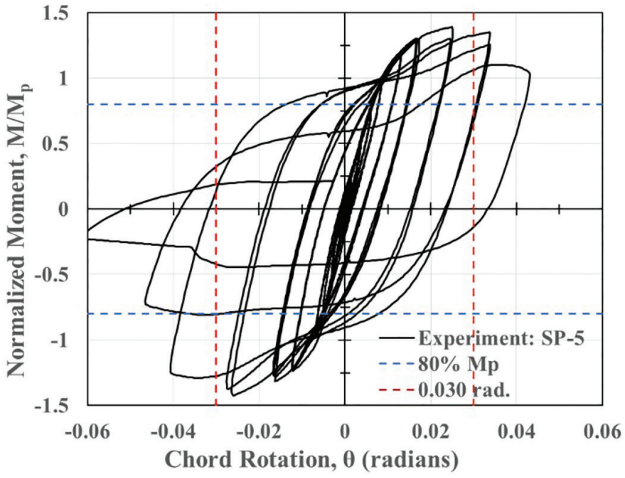

(d) Specimen SP-5

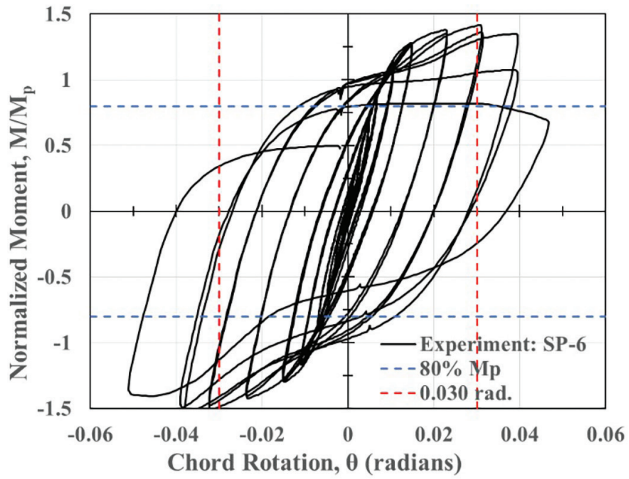

(e) Specimen SP-6

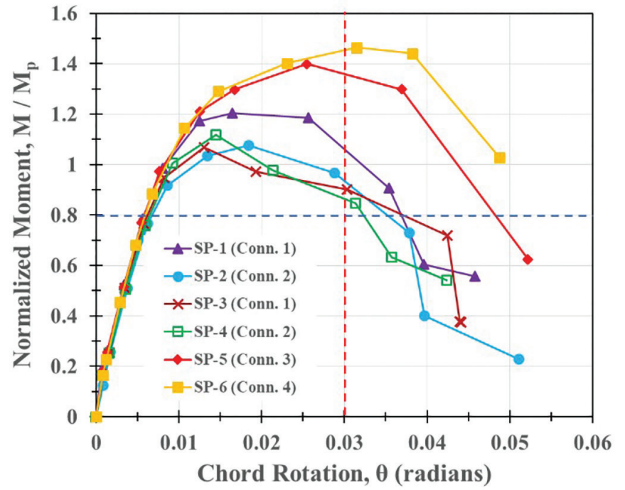

(f) Average backbones of all six specimens

Fig. 16. Normalized moment-chord rotation curves.

based on structural performance requirements and constructability considerations. The structural performance requirements for the connections were to (1) develop the flexural capacity (and associated shear force) of the coupling beams; (2) develop flexural plastic hinges at the connected ends of the coupling beams; and (3) develop chord rotation of at least 0.03 rad before the flexural resistance reduces to less than 80% of the nominal plastic moment capacity, M_p, of the coupling beam. The paper presented the design, details, and experimental evaluation of the cyclic performance of the proposed connections:

1. Connection types 1, 2, and 3 consist of wider beam flange plates going through slots in the wall web plates. Connection type 4 had a narrow beam flange fitted inside the wall thickness.
2. Connection types 1 and 2 had separate web plates for the wall and beam. The beam web plates were lapped and welded to the wall web plates from the outside. Connection types 3 and 4 had continuous web plates for the beam and wall.
3. The difference between the two connection types (1 and 2) was the continuity of the wall flange (closure) plate. The wall flange (closure) plate was interrupted at the connection leading to monolithic concrete in the wall and beam for connection type 1. The wall flange (closure) plate was continuous at the connection leading to interrupted concrete in the wall and beam for connection type 2.
4. Six composite coupling beam-to-composite wall connection specimens representing the four connection types were tested under cyclic loading. These specimens had composite coupling beam clear span-to-depth (L_b/d) ratios of 3.5 or 5.1.
5. Experimental results indicate that all six connections developed and exceeded the plastic flexural capacities (and associated shear force) of the composite coupling beams, calculated using measured material properties. The flexural capacities of the specimens were between 1.05–1.40 times the plastic flexural capacities of the composite coupling beams calculated using measured material properties.
6. All six connection specimens developed rotation capacity (as measured by chord rotation) greater than 0.03 rad before the flexural resistance degraded to 80% of the nominal plastic moment capacity, M_p, of the coupling beams.

In summary, all four connection types satisfied all the structural seismic performance requirements and can be utilized for connecting composite coupling beams to composite plate shear walls in CC-PSW/CF systems.

ACKNOWLEDGMENTS

The research presented in this paper was supported by the Charles Pankow Foundation and the American Institute of Steel Construction. The opinions expressed in the paper belong to the authors alone. The specimens were fabricated and donated by Geiger & Peters. These research results were also summarized and included in part of Professor Amit Varma's 2021 T. R. Higgins lecture titled, "Steel-Concrete Composite Construction: The Best of Both Worlds." The authors acknowledge the significant contributions of the members of the research advisory panel and Bowen Laboratory researchers and technicians.

REFERENCES

AISC (2016), *Seismic Provisions for Structural Steel Buildings*, ANSI/AISC 341-16, American Institute of Steel Construction, Chicago, Ill.

AISC (2022a), *Seismic Provisions for Structural Steel Buildings*, ANSI/AISC 341-22, American Institute of Steel Construction, Chicago, Ill.

AISC (2022b), *Specification for Structural Steel Buildings*, ANSI/AISC 360-22, American Institute of Steel Construction, Chicago, Ill.

AISC (2023), *Steel Construction Manual*, 16th Ed., American Institute of Steel Construction, Chicago, Ill.

ASCE (2016), *Minimum Design Loads and Associated Criteria for Buildings and Other Structures*, ASCE/SEI 7-16, American Society of Civil Engineers, Reston, Va.

ASCE (2022), *Minimum Design Loads and Associated Criteria for Buildings and Other Structures*, ASCE/SEI 7-22, American Society of Civil Engineers, Reston, Va.

ATC (1992), *Guidelines for Cyclic Seismic Testing of Components of Steel Structures*, Applied Technology Council, Redwood City, Calif.

Broberg, M., Agrawal, S., Varma, A., and Klemencic, R. (2023), "Seismic Design Parameters (R, C_d, and Ω_0) for Uncoupled Composite Plate Shear Walls—Concrete Filled (C-PSW/CF)," *Earthquake Engineering and Structural Dynamics*, Vol. 52, No. 10, pp. 3,149–3,170.

Broberg, M., Shafaei, S., Kizilarslan, E., Seo, J., Varma, A.H., Bruneau, M., and Klemencic, R. (2022), "Capacity Design of Coupled Composite Plate Shear Walls/Concrete Filled (CC-PSW/CF)," *Journal of Structural Engineering*, ASCE, Vol. 148, No. 4.

Bruneau, M., Varma, A.H., Kizilarslan, E., Broberg, M.R., Shafaei, S., and Seo, J. (2019), "R-Factors for Coupled Composite Plate Shear Walls/Concrete Filled (CC-PSW/CF)," Final Report, Project #05-17, Charles Pankow Foundation and American Institute of Steel Construction, accessed January 1, 2020.

El-Tawil, S., Fortney, P., Harries, K., Shahrooz, B., Kurama, Y., Hassan, M., and Tong, X. (2010), "Recommendations for Seismic Design of Hybrid Coupled Wall Systems," ASCE, Reston, Va.

Farsi, A., Keshavarzi, F., Pouladi, P., and Mirghaderi, R. (2016), "Experimental Study of a Replaceable Steel Coupling Beam with an End-Plate Connection," *Journal of Constructional Steel Research*, Vol. 122, pp. 138–150.

FEMA (2020), *NEHRP Recommended Seismic Provisions for New Buildings and Other Structures, Volume I: Part 1 Provisions, Part 2, Commentary*, FEMA P-2082-1, Federal Emergency Management Agency, Washington, D.C.

FEMA (2021), *2020 NEHRP Recommended Seismic Provisions: Design Examples, Training Materials, and Design Flow Charts: Volume I: Design Examples*, FEMA P-2192-V1, Federal Emergency Management Agency, Washington, D.C.

Gong, B. and Shahrooz, B.M. (2001), "Concrete-Steel Composite Coupling Beams. I: Component Testing," *Journal of Structural Engineering*, ASCE, Vol. 127, No. 6, pp. 625–631.

Kizilarslan, E., Broberg, M., Shafaei, S., Varma, A.H., and Bruneau, M. (2021a), "Non-Linear Analysis Models for Composite Plate Shear Walls—Concrete Filled (C-PSW/CF)," *Journal of Constructional Steel Research*, Vol. 184.

Kizilarslan, E., Broberg, M., Shafaei, S., Varma, A.H., and Bruneau, M. (2021b), "Seismic Design Coefficients and Factors for Coupled Composite Plate Shear Walls/Concrete Filled (CC-PSW/CF)," *Engineering Structures*, Vol. 244.

Kizilarslan, E. and Bruneau, M. (2023), "Verification of Seismic Response Modification Factors of Uncoupled Composite Plate Shear Walls/Concrete-Filled (C-PSW/CF)," *Journal of Structural Engineering*, ASCE, Vol. 149, No. 6.

Nie, J.G., Hu, H.S., and Eatherton, M.R. (2014), "Concrete Filled Steel Plate Composite Coupling Beams: Experimental Study," *Journal of Constructional Steel Research*, Vol. 94, pp. 49–63.

Shafaei, S., Varma, A.H., Broberg, M., and Klemencic, R. (2021a), "Modeling the Cyclic Behavior of Composite Plate Shear Walls/Concrete Filled (C-PSW/CF)," *Journal of Constructional Steel Research*, Vol. 184.

Shafaei, S., Varma, A.H., and Klemencic, R. (2021b), "Cyclic Lateral Loading Behavior of Composite Plate Shear Walls/Concrete Filled," *Journal of Structural Engineering*, ASCE, Vol. 147, No. 10.

Traut-Todaro, J. (2019), "SpeedCore, Lateral System Innovation for Today's Construction Challenges," *Modern Steel Construction*, AISC, November.

Varma, A.H., Ahmad, M., Shafaei, S., and Bradt, T. (2021), "Seismic Design and Behavior of Composite Coupling Beam-to-C-PSW/CF Connections," Final Report, Project #06-16, Charles Pankow Foundation and American Institute of Steel Construction.

Varma, A.H., Broberg, M., Shafaei, S., and Taghipour, A.A. (2023), *SpeedCore Systems for Steel Structures*, Design Guide 38, AISC, Chicago, Ill.

Varma, A H., Malushte, S.R., Sener, K.C., and Lai, Z. (2014), "Steel-Plate Composite (SC) Walls for Safety Related Nuclear Facilities: Design for In-Plane Forces and Out-of-Plane Moments," *Nuclear Engineering and Design*, Vol. 269, pp. 240–249.

Varma, A.H., Shafaei, S., and Klemencic, R. (2019), "Steel Modules of Composite Plate Shear Walls: Behavior, Stability, and Design," *Thin-Walled Structures*, Vol. 145.